Effects caused by small discrete two-dimensional roughness elements immersed in turbulent boundary layers

By H. H. NIGIM

Faculty of Engineering, Bir Zeit University, West Bank

AND D. J. COCKRELL

Department of Engineering, University of Leicester

In order to determine the downstream consequences of the presence of small discrete surface discontinuities situated on otherwise smooth surfaces and subjected to six equilibrium two-dimensional adverse-pressure-gradient turbulent boundary-layer flows, these conditions were first established in a special-purpose wind tunnel. A surface discontinuity is small if it lies within the logarithmic region of the undisturbed boundary layer. Immediately downstream of such discontinuities flow separation ensues. After the subsequent reattachment, measurements were made of the downstream boundary-layer development. Even in strong adverse pressure gradients the local increments of momentum thickness caused by these roughness elements were well predicted by Gaudet & Johnson's zero-pressure-gradient correlation. With highly adverse pressure gradients it was found that these small surface discontinuities have little influence on the flow downstream. The essential outcome of this work is that the incremental drag of small roughness elements depends solely on local wall variables. Thus, when the pressure gradient is strongly adverse and the local skin friction is correspondingly small, the incremental drag of the roughness element becomes similarly small. After reattachment, it has an insignificant effect on the flow downstream of it.

1. Introduction

For modern fuel-efficient transport aircraft the presence of surface discontinuities, such as remain when auxiliary lifting surfaces are retracted in cruising flight, can have a significant effect on wing design. Often such discontinuities occur in regions of high adverse pressure gradient where the developing boundary layer over the wing is close to separation. Thus there is little margin for error in predicting the aerodynamic characteristics of the wing. The effects of such discontinuities are known if at their location the pressure gradient is small. However, when it is highly adverse so that the shape factor H is of the order of 2.0 or more, the consequences are much less well appreciated.

In the wind tunnel in which these tests were performed six different equilibrium flows were established. Equilibrium flows were chosen both because of their comparative mathematical simplicity and because in adverse pressure gradients the conditions for boundary-layer stability for such flows are much better understood than they are for non-equilibrium flows (Rotta 1962). These flows were then

perturbed by the presence of small surface discontinuities. In subsequent analysis the latter were modelled as if they constituted line discontinuities on surfaces at which step changes occur to the integral parameters of the boundary layer. Once the roughness element drag coefficient has been established the local increase in momentum thickness is directly determined. A step change in displacement thickness will also occur. If the magnitude of these changes is known, integral boundary-layer prediction techniques then enable the flow characteristics downstream to be determined.

Small discrete surface discontinuities will occur in a number of different engineering applications. For example, they could be representative of cooling fins on nuclear fuel elements, roof supports in mine galleries or ridges in river beds. However, in none of these cases is the free-stream pressure gradient so highly adverse as it can be in the transport aircraft application for which these experiments were carried out.

2. Experimental programme

2.1. *Generation of equilibrium boundary layers on a smooth wall*

Criteria to be satisfied. By analogy with laminar self-similar boundary layers an equilibrium turbulent boundary layer is one for which the gross properties of the outer region, constituting some 85–95 % of the total boundary layer, can be scaled with a single parameter such as the boundary-layer defect thickness Δ, where

$$\Delta = \int_0^\infty \frac{U - u}{u_\tau} \, \mathrm{d}y,$$

U denoting the free-stream velocity, u the local velocity distant y from the boundary in a layer of thickness δ and u_τ, the friction velocity, expressed in terms of the local wall shear stress, c_f, by $u_\tau/U = (\tfrac{1}{2}c_f)^{\frac{1}{2}}$. In an equilibrium layer both velocity-defect profiles and shear-stress profiles are self-similar.

This self-similarity of velocity-defect profiles implies, as Clauser (1954) originally demonstrated, that in an equilibrium boundary layer $(U-u)/u_\tau$ is a function of y/δ only. Hence $(U-u)^2/u_\tau^2$ is a similar unique function and thus in such a boundary layer the defect shape factor G, defined as

$$G = \frac{\displaystyle\int_0^\infty \left[\frac{U-u}{u_\tau}\right]^2 \mathrm{d}y}{\displaystyle\int_0^\infty \frac{U-u}{u_\tau} \mathrm{d}y}$$

will be a constant. Through algebraic manipulation the conventional shape factor H, which is the rate of displacement thickness δ^* to momentum thickness θ, can be expressed in terms of the defect shape factor G by

$$H = \frac{\delta^*}{\theta} = \left[1 - \left(\frac{c_f}{2}\right)^{\frac{1}{2}} G\right]^{-1}.$$

This relationship shows that H is only constant in an equilibrium turbulent boundary layer if the local skin fraction c_f is invariant with the distance x over which the boundary layer develops. Rotta demonstrated that this latter condition is necessary if the whole boundary layer, including the logarithmic region, is to be in equilibrium. However, special-purpose surfaces with appropriate roughness distributions are required to achieve it. In practice, therefore, in an equilibrium boundary layer the defect shape factor G remains constant but, depending on the skin-friction coefficient distribution variation, some streamwise variation of the shape factor H will occur.
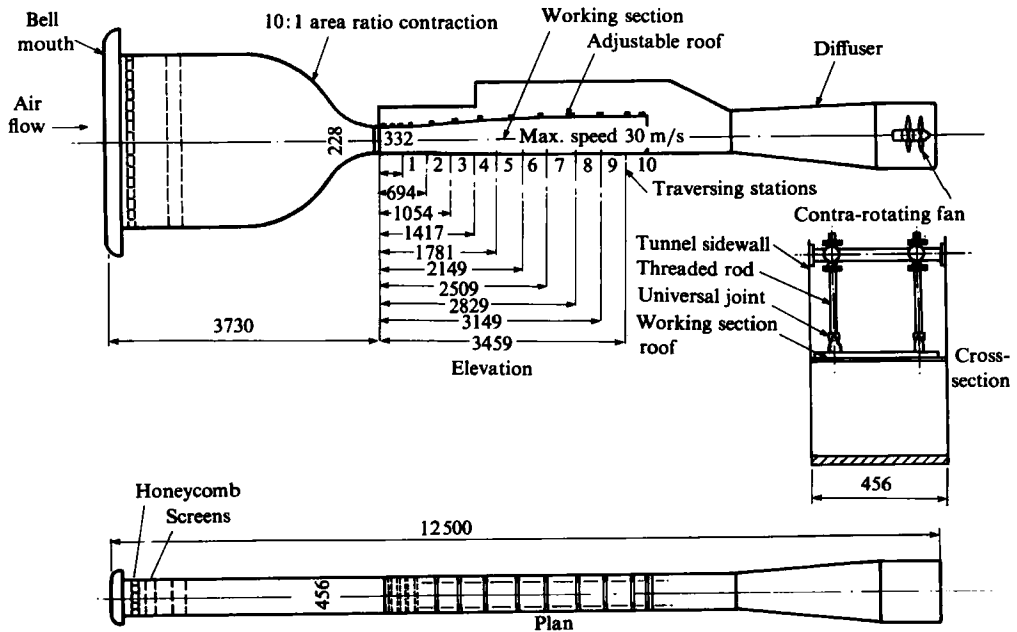
FIGURE 1. Boundary layer wind tunnel. All dimensions in mm.

Clauser also showed that the condition to be satisfied for a turbulent boundary layer to be in equilibrium was the maintenance of a constant value of pressure-gradient parameter β along the developing layer. This parameter, equal to $(\delta^*/\tau_w)\,\mathrm{d}p/\mathrm{d}x$, determines the ratio of the pressure-imposed forces to the shear forces, which together cause the rate of change of momentum in the boundary layer. In practice it has been shown that constancy of β can be assured by maintaining the variation of free-stream velocity U with streamwise distance x in such a way as to satisfy U proportional to x^m, where for a given equilibrium layer m is a constant.

In spite of Rotta's observations, incompressible two-dimensional turbulent boundary-layer flows which are acceptably close to equilibrium can be obtained if the following conditions are satisfied: (i) the shape factor H either remains constant or decreases only very slowly as the momentum thickness-based Reynolds number R_θ increases; (ii) the momentum thickness of the boundary layer grows linearly with streamwise distance x; (iii) the free-stream velocity satisfies the relationship $U \propto x^m$.

Details of the boundary-layer wind tunnel. The boundary-layer tunnel in which six equilibrium flows of increasing pressure adversity were established is shown in figure 1. It has a uniform width of 456 mm and an inlet contraction of 10:1 area ratio. Equilibrium flows having different values of m can be established over the 3.5 m available for boundary-layer development by adjustment of a flexible roof to the working section so that appropriate free-stream velocity distributions are developed. Downstream of the contraction the height of the working section is 228 mm, giving it a 2:1 aspect ratio at inlet.

Characteristics of the flows established. By observing the linear relationship between the momentum thickness and the streamwise distance the commencement of equilibrium was determined from the measured values of momentum thickness, as shown in figure 2. Using these measurements the values of m, given with other equilibrium parameters in table 1, were determined. The required two-dimensionality
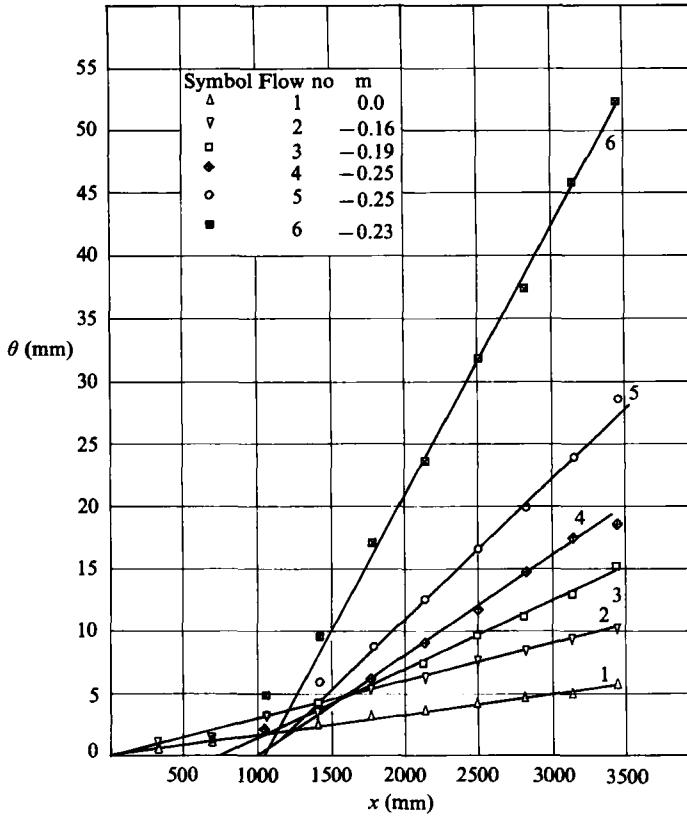
FIGURE 2. Momentum thickness growth for the six equilibrium flows.

Flow number	Symbol used in figures 2 and 6	Description	m (i)	β (ii)	H (ii)	G (ii)	E_τ	E_p	Local skin friction coefficient c_f range
1	△	Zero pressure gradient	0.00	0.0	1.33	6.9	0.021	0.000	$2.7-2.5 \times 10^{-3}$
2	▽	Mild adverse pressure gradient	−0.16	0.7	1.37	8.1	0.015	0.006	$2.5-2.2 \times 10^{-3}$
3	◻	Mild adverse pressure gradient	−0.19	1.7	1.44	10.0	0.010	0.017	$2.2-1.9 \times 10^{-3}$
4	◈	Adverse pressure gradient	−0.25	4.9	1.62	14.6	0.005	0.023	$1.5-1.3 \times 10^{-3}$
5	○	Highly adverse pressure gradient	−0.25	8.2	1.72	18.2	0.003	0.025	$1.1-1.0 \times 10^{-3}$
6	◙	Highly adverse pressure gradient	−0.23	56.7	2.26	40.4	0.001	0.003	$0.4-0.4 \times 10^{-3}$

(i) Two different equilibrium flows can be established for which the same value of exponent m applies.
(ii) Measured values of parameters β, H and G in the equilibrium regions have been averaged, then tabulated.

TABLE 1. Values of equilibrium parameters appropriate to the experimental flows established
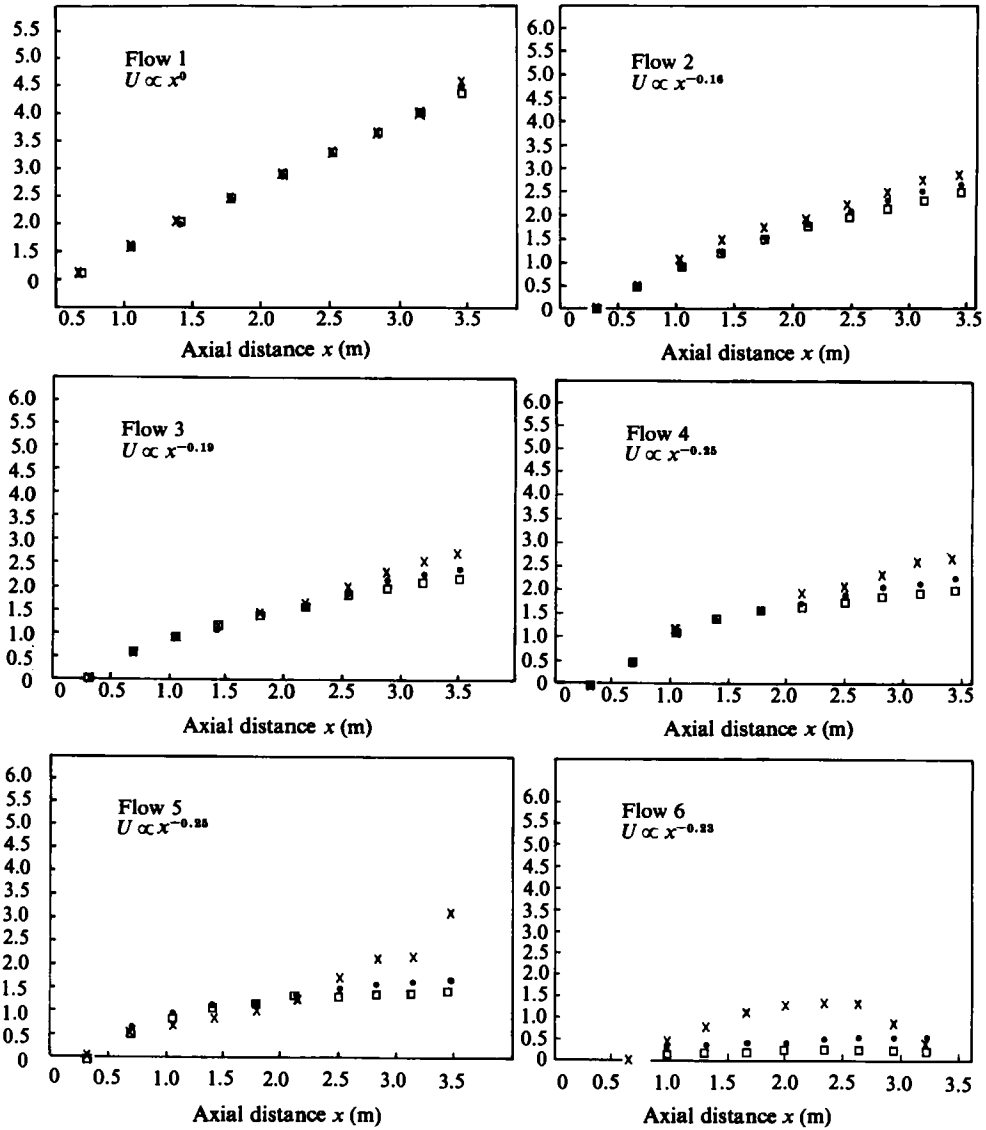
FIGURE 3. Tests of two-dimensionality for the six equilibrium flows by
the integrated von Kármán momentum equation.

Equation left-hand side

$$\times = \frac{[U^2\theta]_x}{[U^2\theta]_{x_0}} - 1 + \frac{1}{2}\int_{x_0}^{x}\frac{\delta^*}{\theta_{x_0}}d\left[\frac{U_x^2}{U_{x_0}^2}\right].$$

Equation right-hand side without and with normal stress terms estimation

$$\Box = \int_{x_0}^{x}\frac{[u^2\tau]_x}{[U^2]_{x_0}}d\left[\frac{x}{\theta_{x_0}}\right], \quad \bullet = \Box + 0.072\left\{\frac{[U^2\theta]_x}{[U^2\theta]_{x_0}} - 1\right\}.$$

of flow was verified both by seeking to satisfy equality between the two sides of the
integrated von Kármán momentum equation, as described by Coles & Hirst (1969),
and also by determining the deviation in the wake flow resulting from two needles,
mounted at an upstream position on the wind-tunnel floor. Results of the first
technique are shown in figure 3. When appropriate estimations for normal stress
terms, as suggested by East, Sawyer & Nash (1979), have been included these are
considered to be satisfactory. The needle-wake technique, suggested to the authors
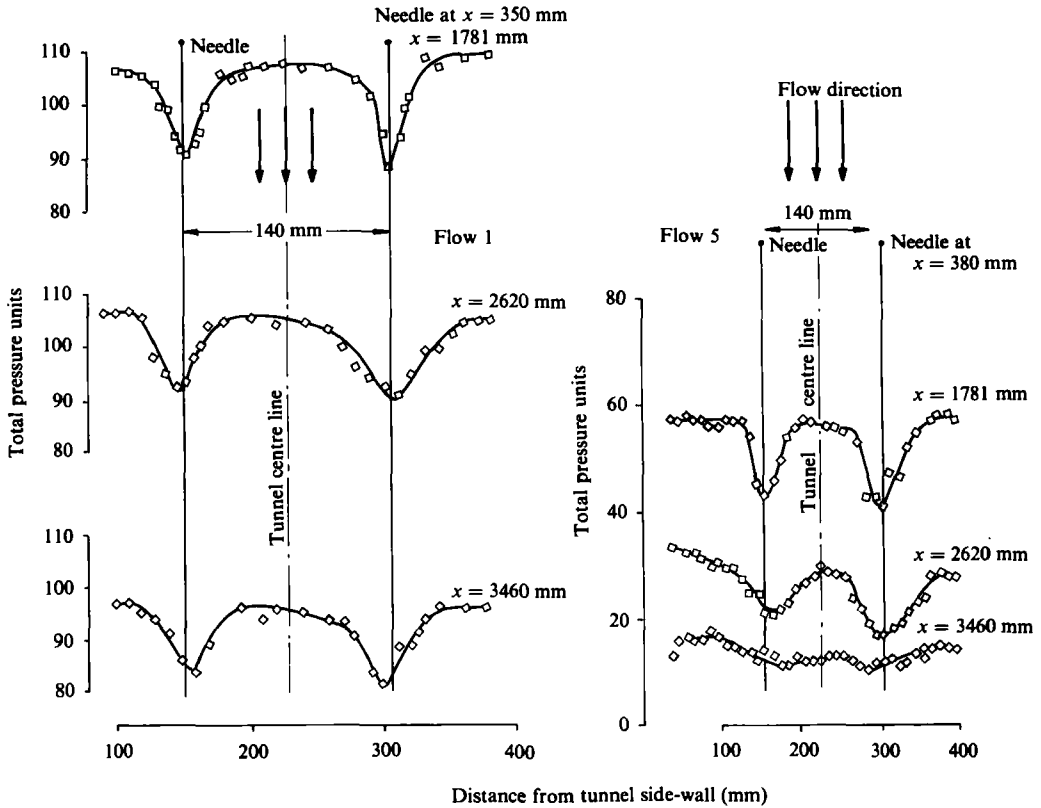
FIGURE 4. Examples of the needle-wake technique for assessment of flow two-dimensionality for flow 1 and flow 5. Symbols indicate the spanwise variation of total pressure 60 mm above the surface.

by K. G. Winter of the Royal Aircraft Establishment, Bedford, is highly sensitive. Examples showing its use for the zero-pressure-gradient flow (flow 1) and for the highly adverse pressure-gradient case (flow 5) are given in figure 4.

The universality of the velocity profiles obtained with these equilibrium boundary layers is indicated in the velocity-defect graphs of figure 5. Their skin-friction coefficients and their shape parameters are shown in figure 6, while their equilibrium loci, in generalized coordinates, together with experimental results by Bradshaw (1967) and by Good & Joubert (1968) are given in figure 7. This equilibrium locus derives from East, Smith & Merryman's (1977) parameters, $E_f = G^{-2}$ and $E_p = \beta/G^2$. In highly adverse pressure gradients E_f and E_p (where subscripts f and p denote friction and pressure gradient respectively) are more appropriate than G since

$$G = \left(1 - \frac{1}{H}\right)\left(\tfrac{1}{2}c_f\right)^{\frac{1}{2}}$$

and, as c_f tends to zero, G tends to infinity. E_f and E_p were subsequently linearly related empirically by East, Sawyer & Nash as

$$E_f = 0.024 - 0.8E_p.$$

This relationship is also shown in figure 7.
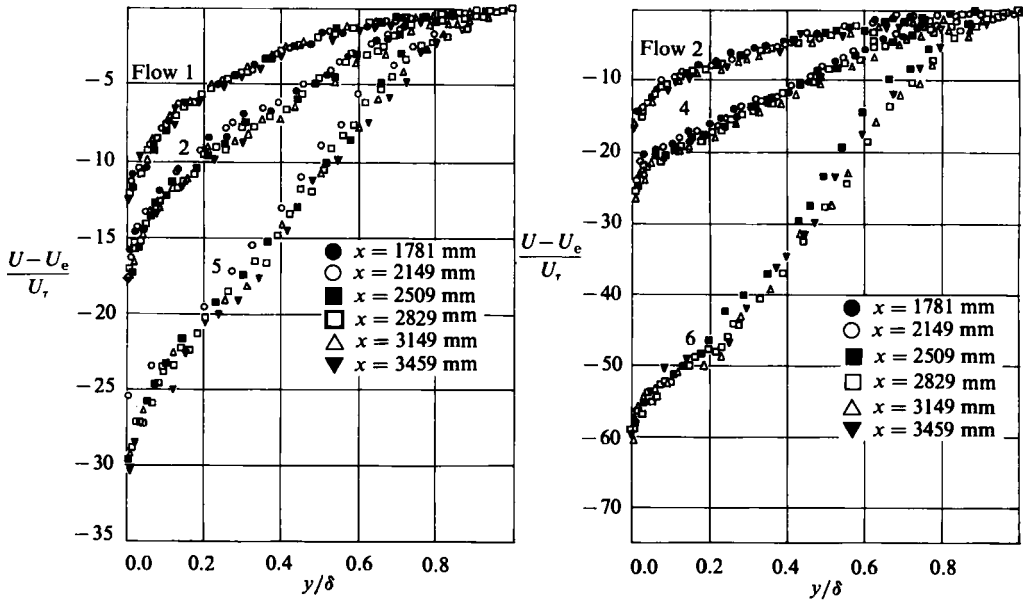
FIGURE 5. Velocity defect profiles for the six equilibrium flows.
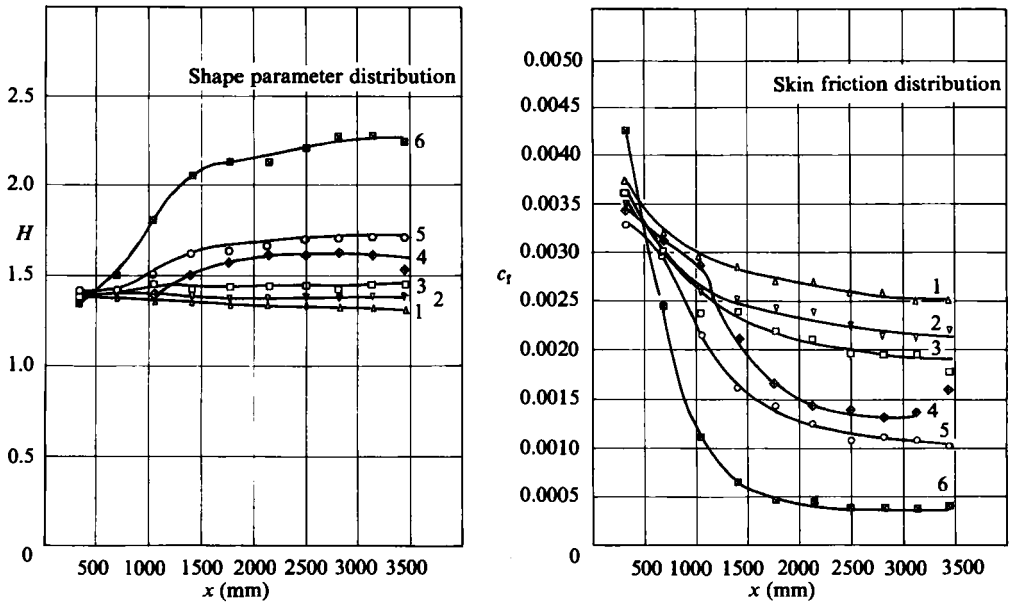
FIGURE 6. Variation of shape parameter H and local skin friction
coefficient c_f for the six equilibrium flows.

2.2. *Experiments with roughness elements*

Roughness element shapes. The shapes and sizes of the roughness elements tested are listed in table 2. For the major part of the programme the elements used were constructed from square-sectioned steel strip which entirely spanned the wind, tunnel working section and which varied in linear dimension from 3.2 mm to 12.7 mm. The size adopted in any experiment varied with the flow characteristics in such a way that these elements lay within the boundary-layer logarithmic region and thus could be categorized as small.
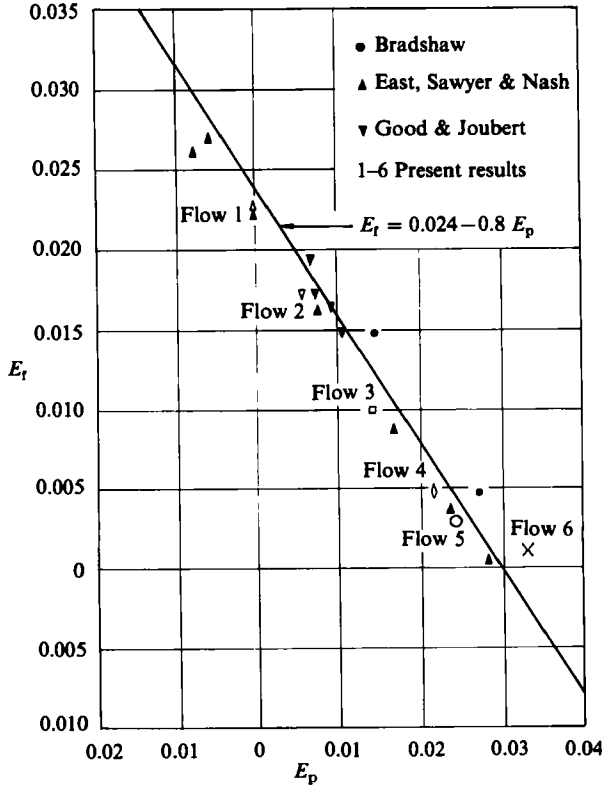
FIGURE 7. Equilibrium loci shown in the generalized coordinates E_t and E_p.

Flow number	Roughness-element location, x (mm) (see figure 2)	Clean-surface boundary-layer thickness at x, δ (mm)	Roughness-element cross-sectional shape	Height of element h (mm)				
				3.18	4.77	6.35	9.53	12.70
1	1781	37.5	Square	√	√	√	√	√
2	1417	43.8	Square	√	√	√	√	—
3	1620	44.8	Square	√	√	√	√	—
4	1620	63.5	Square	√	√	√	√	—
5	2020	95.4	Square	√	√	√	—	—
	2710	120.8	Triangular right-angled (see figure 10)	—	—	√	—	—
6	2310	190.6	Square	—	—	√	√	√
	2310	190.6	Triangular right-angled (see figure 10)	—	—	—	√	—

TABLE 2. Roughness-element shapes tested

In highly adverse pressure-gradient flows a more limited series of experiments was also performed on triangular-section small roughness elements. Equiangular and right-angled shapes were tested, the latter with both the ramp and the step facing upstream. Only the right-angled shapes are considered in table 2 and figure 10.

Methods used to measure drag. Three techniques are available for the measurement of roughness element drag. A direct method using skin friction balances was adopted by Wieghardt (1942), Winter & Gaudet (1967), Gaudet & Johnson (1970), Gaudet & Winter (1973) and Pallister (1974). A semi-direct method in which pressure distributions over the elements were determined and integrated to obtain element drag was used by Good & Joubert, by Lacey (1974) and by Pallister. In the present programme of work, following earlier experimental measurements by Lacey and by Abd Rabbo (1976) at Leicester University, the drag was determined by momentum-defect methods. With this technique, the boundary-layer momentum thickness is first measured over the clean surface on which the roughness element will be located. Next, having attached the roughness element to the surface, the local increase in momentum thickness $\Delta\theta$ is determined. For the purpose of downstream flow prediction it is desirable to model the effect of the roughness element on the flow as if at its location it caused abrupt changes to the boundary-layer characteristics. However, since the element provokes local flow separation, its gross effects extend over a number of element height lengths immediately downstream. Thus, even if it were straightforward to measure the disturbed momentum thickness of the boundary layer immediately downstream, this measurement would be meaningless as it would not account for any change in flow characteristics which occurred in the separation regime downstream of the element.

The procedure adopted, therefore, to determine $\Delta\theta$ was to measure the disturbed boundary-layer momentum thickness at a number of downstream locations and extrapolate upstream the resulting experimental relationship between momentum thickness and distance. Examples of this upstream extrapolation technique are shown in figure 8. In practice, except in highly adverse pressure gradients, it was found to be well represented by upstream application of the Nash & Bradshaw (1967) magnification factor relationship

$$\frac{\Delta\theta}{\Delta\theta_0} = \left(\frac{\theta_0}{\theta}\right)^{0.2}\left(\frac{U_0}{U}\right)^{4.2},$$

where $\Delta\theta$ is the increased momentum thickness at a downstream traverse station caused by the roughness element and measured there, U is the free-stream velocity at that downstream location and θ is the clean-surface momentum thickness there. The subscript o denotes the roughness element location.

Since the element has been modelled as if it were of negligible thickness its drag $D = \frac{1}{2}\rho U^2 h$ is given by $\rho U^2 \Delta\theta_0$ regardless of any external pressure gradient. Hence the drag coefficient C_D is equal to $2\Delta\theta_0/h$, where h is the element height.

These three measurement techniques determine different quantities. Whereas the pressure-distribution method neglects any change of skin friction caused by the element, the pressure measurements made are direct; thus the accuracy in determining the roughness-element drag mainly depends on the number and disposition of the pressure tappings that can be accommodated in the element. The skin-friction balance method only includes those changes which are accommodated on the floating-element balance plate and measurements are therefore functions of the size of that plate. The momentum-defect technique includes all such effects as are present within the control volume bounded by the roughness element and the downstream traverse station, but when the changes in momentum thickness brought about by the roughness element
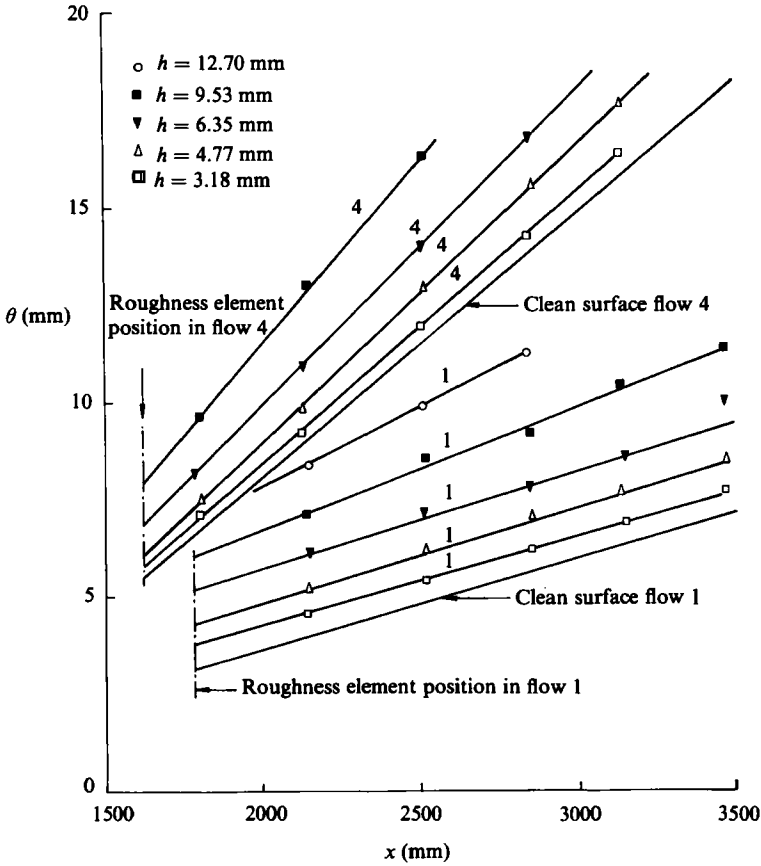
FIGURE 8. Upstream extrapolation of boundary-layer momentum thickness measurement in the presence of roughness elements. Flows 1 and 4.

are quite small, as they are if these surface irregularities are small or in strong adverse pressure gradients, the uncertainty of evaluation can be high. It is a necessary limitation of this upstream extrapolation technique for the height of such roughness elements compared to local boundary-layer thicknesses to be sufficiently small for the perturbations which they cause to the downstream flow to be weak, provoking no significant change to the turbulence structure in the downstream boundary layer. Surface irregularities which cause weak flow perturbations are categorized as small by Bradshaw & Wong (1972), to distinguish them from medium-sized and large surface irregularities which respectively significantly change the turbulence structure or mutate the boundary layer into a wake or a mixing layer.

Following Good & Joubert, for surface discontinuities of height h which are sufficiently small for their drag D to be independent of the free-stream velocity, if

$$D = f(\text{discontinuity shape}; h; u_\tau; \rho; \mu),$$

then

$$\frac{D}{\rho u_\tau^2 h} = \frac{C_D}{c_f} = F(\text{discontinuity shape}, h^+),$$

where the roughness-element drag coefficient $C_D = D/\frac{1}{2}\rho U^2 h$, the clean-surface skin-friction coefficient $c_f = \tau_\omega/\frac{1}{2}\rho U^2 = 2(u_\tau/U)^2$ and $h^+ = hu_\tau/\nu$. In establishing
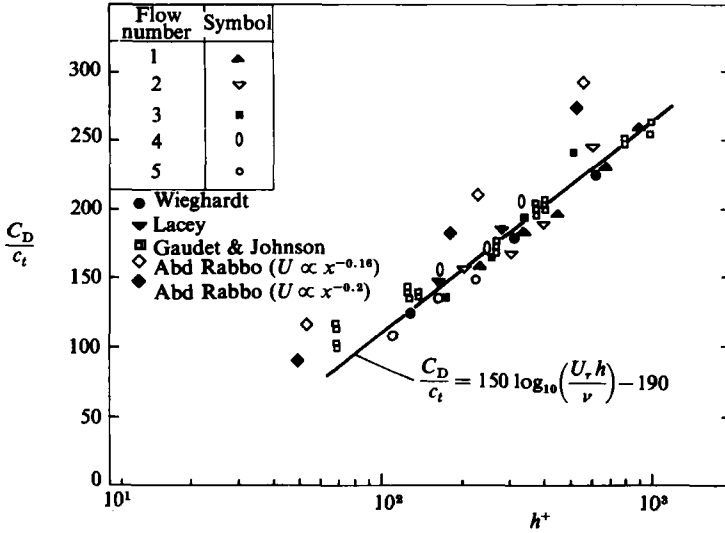
FIGURE 9. The drag of isolated small square roughness elements
in adverse-pressure-gradient flows.

law-of-the-wall similarity parameters for fences within the logarithmic region, Good
& Joubert anticipated that any pressure-gradient effects would be negligibly small.
However, the results of their experiments indicated that there was some dependence,
with no very obvious trend. This they attributed to a variation with the free-stream
pressure gradient of the base pressure immediately downstream of the element.

Thus, for a given discontinuity shape in a constant dimensionless pressure gradient,
C_D/c_f may be expressed as a function of the friction height h^+ only. Outside the
logarithmic region C_D/c_f will be independent of molecular viscosity and hence the
functional relationship must be logarithmic. Hence

$$\frac{C_D}{c_f} = A \log_{10} h^+ + B,$$

the constants A and B depending on the roughness-element shape.

Results of the drag measurements. Drag characteristics of small isolated square
roughness elements are shown in figure 9. Contrary to Good & Joubert's experience,
no pressure-gradient dependence is detectable but, as figure 7 indicates, in the present
test programme the range of pressure-gradient adversity is much more extensive than
that adopted by Good & Joubert. The differences between their results with different
pressure gradients do not appear to be systematic and, at least for fence heights which
lie within the logarithmic region of the boundary layer and are therefore comparable
to the surface discontinuities examined in this present study, probably lie within the
range of experimental error.

When the free-stream pressure gradient is strongly adverse, as in flows 5 and 6,
it is the height rather than the shape of the roughness element which is most
significant in determining its drag characteristics. This is illustrated in figure 10 where
it is shown that, at large distances downstream of elements of the same height but
differing shape, differences in integral boundary-layer characteristics are not
significant. However, with a zero-free-stream pressure gradient Winter & Gaudet
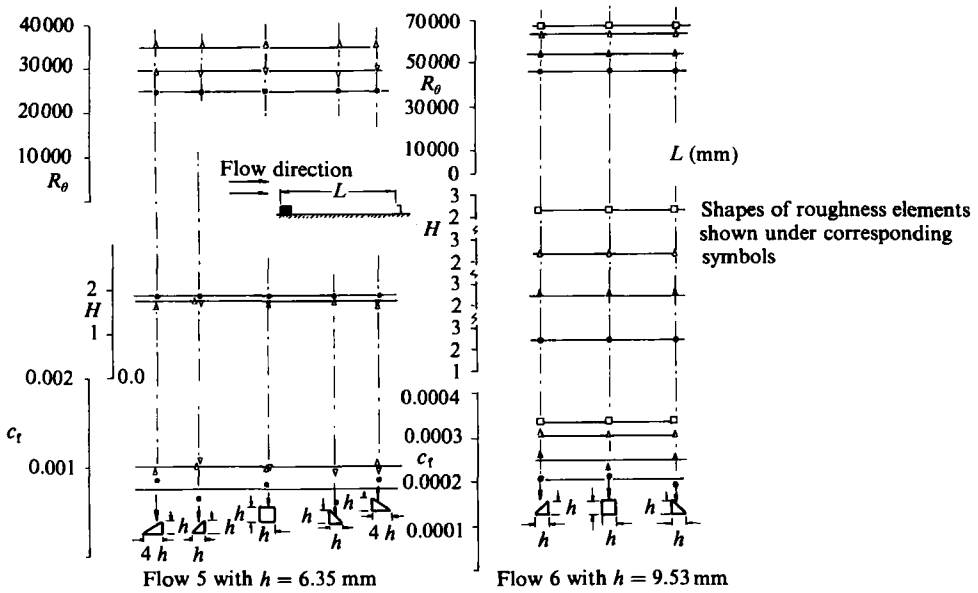
FIGURE 10. Flow characteristics downstream of roughness elements of similar height but varying shape when the external pressure gradient is highly adverse: ●, $L = 120$; ▽, 400; ▲, 440; △, 750; ○, 1070 mm. Shapes of roughness elements are shown under corresponding symbols.
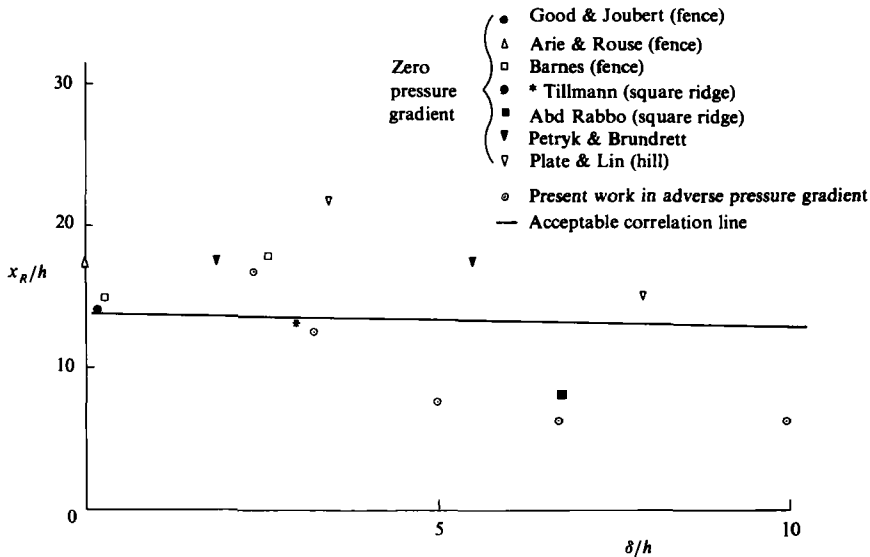
FIGURE 11. Variation of downstream flow separation length x_R with boundary-layer thickness to roughness-height ratio, δ/h.

have shown that the roughness element shape does have a significant effect upon its drag.

Local separation downstream of the elements. In figure 11 experimental results are shown from a variety of sources for the dimensionless reattachment length x_R/h' measured behind discrete surface elements of varying shapes. Eaton & Johnston (1981) have shown that this reattachment length is a function of a number of parameters which describe:

(i) the flow characteristics at the obstacle location;

(ii) the free-stream pressure gradient; and

(iii) possible blockage of the wind tunnel by the element.

It has been demonstrated (de Brederode & Bradshaw 1972) that the latter is unlikely to be a significant parameter if the ratio of the wind-tunnel width to element height exceeds 10:1.

The flow characteristics of the location of the element are represented in this figure by the boundary-layer thickness to roughness-height ratio, δ/h. Other significant parameters proposed by Eaton & Johnson are the boundary-layer momentum-thickness Reynolds number at this location and the free-stream turbulence intensity. Thus, in this figure the scatter is evident. Keuhn (1980) has shown that there is an increase in reattachment length with adversity of pressure gradient; however, this observation is dependent on the size of the roughness element. Where it lies within the logarithmic region the measurements shown in figure 11 made behind different height elements subjected to a highly adverse pressure gradient (flow 6) suggest no obvious external pressure-gradient effect. Thus for small roughness elements an acceptable correlation line, drawn in figure 11 with considerable experimental scatter which has probably been caused by the unspecified clean-surface flow characteristics, shows an independence of free-stream pressure gradient.

3. Discussion

For discrete roughness elements which are sufficiently small for their friction height to lie within the logarithmic boundary layer, the relationship developed by Gaudet & Johnson for zero-pressure-gradient flows,

$$\frac{C_D}{c_f} = 150 \log_{10} h^+ - 190,$$

is seen in figure 9 to be valid for all pressure gradients. This figure includes results obtained by Wieghardt and by Lacey on small ridges in zero pressure gradients as well as some results which were obtained by Abd Rabbo in adverse pressure gradients.

On a clean surface, at a point at which a roughness element is to be located, the skin-friction coefficient decreases in value significantly with the adversity of pressure gradient. Since it is shown that the relationship for roughness-element drag coefficient is universally valid, the latter must also decrease and its effect on the flow downstream of it will therefore diminish. It is thus seen that when flows over clean surfaces tend to separate under the influence of strongly adverse pressure gradients the effect of small isolated surface irregularities is of much less significance than when the pressure gradient is less severe. There is no reason to limit this observation to the equilibrium flows which were examined experimentally. The result also applies to non-equilibrium flows.

This is contrary to general expectation. It might be anticipated that when a flow is about to separate from a clean surface the presence of a small surface irregularity could be enough to complete this process. However, if this irregularity is sufficiently small for it to lie within the logarithmic region, it is readily demonstrated that this expectation is not fulfilled.

Consider, for example, an isolated roughness element of dimensionless height h^+ equal to 600 on a surface at zero pressure gradient and then on a surface over which the free-stream pressure gradient is highly adverse. In air at sea level, at a free-stream velocity of 100 m s^{-1} the element would be of about 2.5 mm height in the first instance, 5.5 mm height in the second. The corresponding values of its drag per unit width would be some 15 newtons and 34 newtons respectively. Yet the increase in

boundary-layer momentum thickness which each would cause amount to about 0.74 mm and 0.30 mm. The experiments described here show that the original clean-surface momentum thickness was of the order of 2.5 mm and 11 mm respectively, that is, in a highly adverse pressure gradient a square-sectioned roughness element of some 5.5 mm height causes only some 3 % local increase in momentum thickness, an increase which would have little effect on downstream flow characteristics. In any case, this increase is within the experimental uncertainty of the measurement techniques which have been described.

4. Conclusions

Provided that isolated two-dimensional roughness elements are small enough to be accommodated within the logarithmic region of the boundary layer developed on a smooth surface, i.e. h^+ is somewhat less than 1000, the drag of those elements can be represented by a universal logarithmic relationship regardless of the external pressure gradient.

Two important consequences of this relationship are that when the external pressure gradient is adverse it is the height rather than the cross-sectional shape of the element which is the significant parameter, and that whatever its shape may be its downstream effect decreases in significance with the adversity of this pressure gradient. Thus, if the flow is about to separate from a clean surface subject to a highly adverse pressure gradient the presence of such a roughness element will not greatly assist this separation process.

REFERENCES

ABD RABBO, M. F. 1976 Aerodynamic drag of ridge arrays in adverse pressure gradients. Ph.D. Thesis, Univ. of Leicester.
ARIE, M. & ROUSE, H. 1956 *J. Fluid Mech.* 1, 129.
BARNES, C. S. 1965 CP863, Aeronautical Research Centre 26, 677.
BRADSHAW, P. 1967 *J. Fluid Mech.* 29, 625.
BRADSHAW, P. & WONG, F. Y. F. 1972 *J. Fluid Mech.* 52, 113.
DE BREDERODE, V. & BRADSHAW, P. 1972 *Imperial College Aero. Rep.* 72-19.
CLAUSER, F. H. 1954 *J. Aero. Sci.* 21, 91.
COLES, D. E. & HIRST, E. A. (eds) 1969 *Proceedings Computation of Turbulent Boundary Layers, Vol. II, 1968 AFOSR-IFP – Thermosciences Division Stanford University.*
EAST, L. F., SAWYER, W. G. & NASH, C. R. 1979 *Royal Aircraft Establishment Tech. Rep.* 79040.
EAST, L. F., SMITH, P. D. & MERRYMAN, P. J. 1977 *Royal Aircraft Establishment Tech. Rep.* 77046.
EATON, J. K. & JOHNSTON, J. P. 1981 *AIAA J.* 19, 1093.
GAUDET, L. & JOHNSON, P. 1970 *Royal Aircraft Establishment Tech. Rep.* 70190.
GAUDET, L. & WINTER, K. G. 1973 *AGARD Conf. Proc.* 124, Paper No. 4.
GOOD, M. C. & JOUBERT, P. N. 1968 *J. Fluid Mech.* 31, 547.
KEUHN, D. M. 1980 *AIAA J.* 18, 323.
LACEY, J. 1974 The aerodynamic drag of square ridges. M.Sc. Thesis, Univ. of Leicester.
NASH, J. F. & BRADSHAW, P. 1967 *J. R. Aero. Soc.* 71, 44.
PALLISTER, K. C. 1974 *Aircraft Research Association Rep.* 37.
PETRYK, S. & BRUNDRETT, E. 1967 *Waterloo Univ. Mech. Engng Res. Rep. No. 4.*
PLATE, E. J. & LIN, C. W. 1964 Colorado State Univ. CER-65-EJP-14, AD-614067.
ROTTA, J. C. 1962 *Prog. Aero Sci.* 2, 5.
TILLMANN, W. 1945 Zentralle Wissenschaftliche Berifte U & M 6627 [English transl. Ministry of Aircraft Production-VG-34-45T].
WIEGHARDT, K. 1942 Zentralle Wissenschaftliche Berifte FB 1563.
WINTER, K. G. & GAUDET, L. 1967 *Royal Aircraft Establishment Tech. Memo. Aero* 1005.